

REPORT DOCUMENTATION PAGE

Form Approved
OMB No. 0704-0188

Public reporting burden for this collection of information is estimated to average 1 hour per response, including the time for reviewing instructions, searching existing data sources, gathering and maintaining the data needed, and completing and reviewing the collection of information. Send comments regarding this burden estimate or any other aspect of this collection of information, including suggestions for reducing this burden, to Washington Headquarters Services, Directorate for Information Operations and Reports, 1215 Jefferson Davis Highway, Suite 1204, Arlington, VA 22202-4302, and to the Office of Management and Budget, Paperwork Reduction Project (0704-0188), Washington, DC 20503.

1. AGENCY USE ONLY (Leave Blank)	2. REPORT DATE	3. REPORT TYPE AND DATES COVERED	
	February 2001	Final; 01 December 1996 through 21 February 2001	
4. TITLE AND SUBTITLE Basic Research into High-Speed Supercavitating Bodies			5. FUNDING NUMBERS G; N00014-97-1-0126
6. AUTHORS David R. Stinebring			
7. PERFORMING ORGANIZATION NAME(S) AND ADDRESS(ES) Applied Research Laboratory The Pennsylvania State University PO Box 30 State College, PA 16804-0030			8. PERFORMING ORGANIZATION REPORT NUMBER
9. SPONSORING / MONITORING AGENCY NAME(S) AND ADDRESS(ES) Office of Naval Research, Code 333 Ballston Centre Tower One 800 North Quincy Street Arlington VA 22217-5660			10. SPONSORING / MONITORING AGENCY REPORT NUMBER
11. SUPPLEMENTARY NOTES			
12a. DISTRIBUTION / AVAILABILITY STATEMENT Approved for Public Release		12b. DISTRIBUTION CODE	
13. ABSTRACT (Maximum 200 words) Critical technologies related to SCAT development, including cavitator hydrodynamics, control surface hydrodynamics, static pressure sensing, flow noise calculations and hydrodynamics modeling of high-speed supercavitating flows. Focused on critical technologies related to SCAT development, including hydrodynamics of advanced cavitator concepts, control surface hydrodynamics, cavity geometry studies for comparison with CFD modeling, small-scale model design and fabrication, and flow noise testing and modeling.			
14. SUBJECT TERMS High-speed supercavitating bodies SCAT hydrodynamics			15. NUMBER OF PAGES 32
			16. PRICE CODE
17. SECURITY CLASSIFICATION OF REPORT unclassified	18. SECURITY CLASSIFICATION OF THIS PAGE unclassified	19. SECURITY CLASSIFICATION OF ABSTRACT unclassified	20. LIMITATION OF ABSTRACT unlimited

NSN 7540-01-280-5500

Standard Form 298 (Rev. 2-89)
Prescribed by ANSI Std. Z39-1
298-102

20011102 017

**Final Report
Basic Research Into High-Speed Supercavitating Bodies
ONR Project N00014-97-1-0126**

By
David R. Stinebring
Applied Research Laboratory
The Pennsylvania State University
P.O. Box 30
State College, PA 16804

This report documents the work for ONR Project N00014-97-1-0126, and is arranged according to time periods covered by each year's funding.

Period of 1 December 1996 to 30 November 1997

The ONR 6.1 basic research for the time period of 1 December 1996 to 30 November 1997 focused on critical technologies related to SCAT development, including, cavitator hydrodynamics, control surface hydrodynamics, static pressure sensing, flow noise calculations and hydrodynamics modeling of high-speed supercavitating flows.

Cavitator model testing was conducted in both the ARL Penn State 48-inch diameter and 12-inch diameter water tunnels. Four large cavitators were tested in the 48-inch tunnel using a specially designed model; a 4.75-inch diameter, 20-degree half-angle cone, a 4.5-inch diameter disk, a 4.5-inch diameter spherical/ring cavitator and a 4.5-inch diameter ogive/ring cavitator. The models were run at speeds up to 45ft/sec with gas ventilation flowrates of up to 360 cu ft/sec measured at cavity pressure. The objectives of this test were to investigate cavity stability for large cavitators at high gas flow rates and to measure tunnel blockage effects with large cavities. One finding was that the boundary layer separation location for the ring cavitators appears to have a significant effect upon the cavity stability.

The model for testing cavitators in the 12-inch diameter water tunnel is shown in Figure 1. The model has lift and drag force cells, cavity ventilation, cavitator water ingestion and, with small modification, will allow gas or steam to be exhausted at the rear of the model into the cavity. Water ingestion through the cavitator can not be run with the force cells in place at the present time. Conical noses and spherical/ring cavitators have been run, with Figure 1 showing a lifting ring cavitator at 13 degrees angle of attack with water ingestion while ventilating the cavity.



Figure 1: Test of a Lifting Ring Cavitator With Water Ingestion, 30 ft/sec-10 psia Pressure

utilized for increased body stability for a SCAT. At the present time only forces parallel to the free stream, lift and drag, are being measured. The supercavitating control surface tests are all being conducted in the 12-inch diameter tunnel. A simulated body cavity is generated along a segment of the tunnel wall by ventilating a wedge shaped step. The stability of this 'body' cavity is a function of Froude number and cavitation number. Control surfaces with wedge half-angles of 7.5 to 10-degrees are being tested at a number of leading edge sweepback angles. This sweepback changes the effective wedge angles with

respect to the free stream. The distortion of the constant pressure surface of the cavity due to the pressure gradient along the wedge pressure side is shown in Figure 2. This change in flow over the wedge can create an increase in the force perpendicular to the free stream, which can be

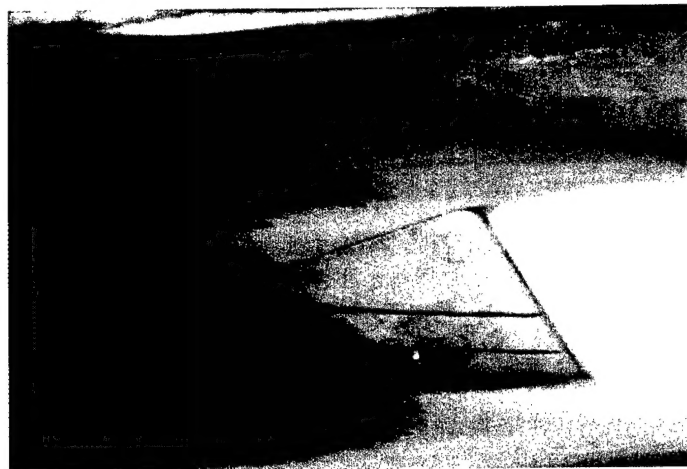


Figure 2: Supercavitating Control Surface Test Showing Cavity Distortion Due to Wedge Pressure Gradient, 40 ft/sec, 10 psia Tunnel Pressure

Calculations have been performed for both natural and ventilated cavity flows over axisymmetric bodies. In the former case, an early implementation of the phase equation gave qualitatively reasonable comparisons with the limited experimental data that is available for the flow over a 45-degree cone-cylinder configuration. Currently, the numerical approach is being refined and is being applied to this configuration. A ventilated cavitation demonstration calculation was performed with an alternative "two-species" formulation. The results indicate that the phase equation approach is preferable and, hence, recent efforts have focused on the phase equation implementation. A critical aspect of a ventilated cavity model is its ability to maintain a stable gas stream in regions where the local pressure is above the cavitation pressure. The present formulation has this capability, while other recently developed cavitation models are not applicable without significant modification.

The acoustics task has focused on analysis and testing of the flow and noise characteristics of the ultra-high-speed water tunnel. Test section boundary layer characteristics at speeds up to 200 ft/sec were obtained through CFD calculations. Turbulent boundary layer wall pressure fluctuations i.e., flow noise, spectra were computed for corresponding test conditions. A transducer mounted flush with the tunnel test section was used to sense the unsteady pressure field. A LC-10 hydrophone mounted in the tunnel settling section served as a sound projector and allowed an assessment of the radiation-field sensitivity of the flush-mounted pressure transducer.

Period of 1 December 1997 to 30 November 1998

The ONR 6.1 basic research for the time period of 1 December 1997 to 30 November 1998 focused on critical technologies related to SCAT development, including

hydrodynamics of advanced cavitator concepts, control surface hydrodynamics, cavity geometry studies for comparison with CFD modeling, small-scale model design and fabrication, and flow noise testing and modeling.

During this past year, advanced cavitator concepts were investigated, including disk-ring, wedge- ring, and variable cavitators. It was shown that the boundary layer separation from the forward section of a ring cavitator affects the cavity stability. A laser light sheet was used for visualization of the boundary layer separation from the spherical section of a disk-ring cavitator and reattachment on the disk. Interacting vortices were seen in the

separated region. It was shown previously that disk-ring cavitators with spherical center elements have high drag. Wedge-ring cavitators, with spherical center elements and having lower drag coefficients, were tested for a range of wedge angles, wedge tilt angles, and flow conditions. Figure 3 shows a ventilated cavity formed by a 45-degree (side angle) wedge-ring cavitator. Variable cavitators can change the drag and thus the cavity size by movement of the center element. Variable cavitators that will allow water ingestion and variable lift have been designed and will be tested.

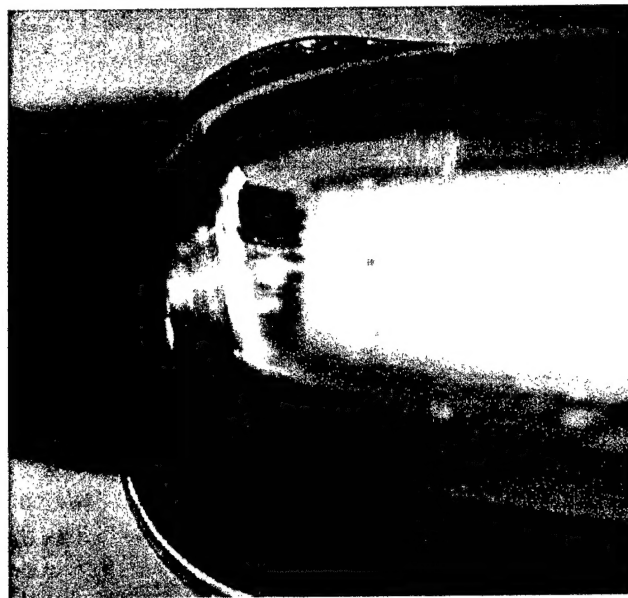


Figure 3: Water tunnel test of wedge-ring cavitator with ventilated cavity

Figure 4 shows some of the supercavitating control fins tested in the 12-inch diameter water tunnel together with the fin mount. During the past year, the transition between the base, partial and supercavitating flow regimes was investigated as a function of wedge half-angle, leading edge sweepback angle and flow incidence angle. The pressure gradient along the pressure surface distorts the cavity wall and changes the relative flow direction.

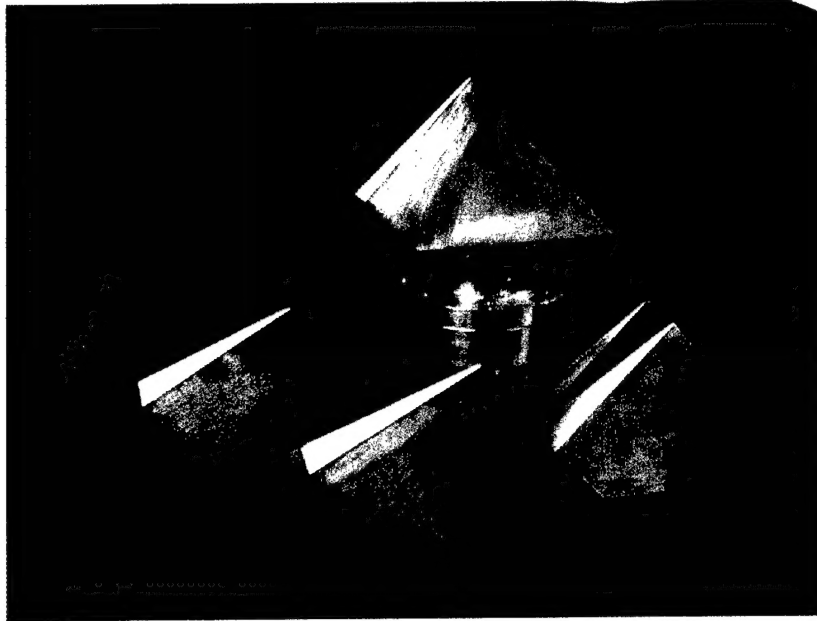


Figure 4: Photograph of supercavitating control surfaces tested in the 12-inch diameter water tunnel- wedge half-angles of 7.5 and 10 degrees with 25, 45 and 65 degree sweepback angles

When the relative flow direction is close to the effective wedge angle, it creates what is known as partial cavitation. In the partial cavitating flow regime there is an unsteady cavitation that causes very high unsteady lift and drag forces. For practical applications, the partial cavitating flow regime should be avoided.

An ONR 6.1 CFD effort is underway at ARL to complement the experimental program. Experiments are being conducted for comparison with the CFD results. Shown in Figure 5 is an 8-inch diameter 8-foot long model to be tested in the water tunnel, together with the computational grid for the model/tunnel. The CFD code will be used to calculate the cavity geometry including the tunnel blockage, wall boundary layer, and three-dimensional buoyancy effects. In another test to investigate cavity geometry, a lifting cavitator, supported on the fully wetted region to minimized cavity disturbances, was run in the 12-inch diameter water tunnel. The rollup of the twin vortices was significantly influenced by the cavitator lift force and lift force direction.

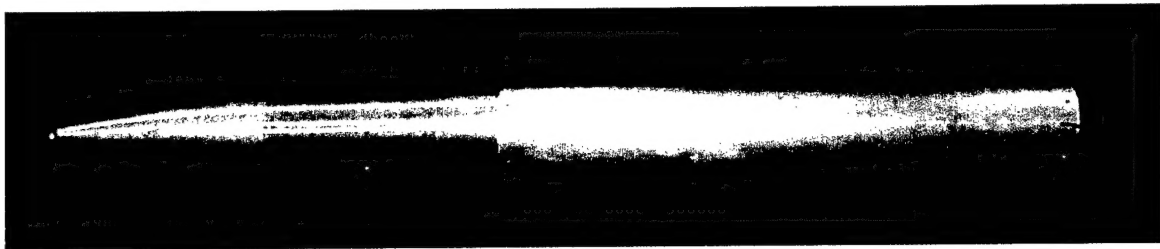


Figure 5: Photograph of 8-inch diameter 8-foot long model to be tested in the 48-inch diameter water tunnel and computational grid for the model in the tunnel

Figure 6 shows the low cost powered model being designed and built to investigate propulsor/ cavity interactions, body/cavity interactions and high-speed flow noise. The model is 4 inches in diameter and 5 feet long and is powered by either hybrid, up to 259 lb-s total impulse, or conventional, up to 337 lb-s, motors. With the higher impulse motors, speeds of up to 250 ft/s should be possible. The outer shell is being manufactured of wound graphite fiber composite using the ARL Penn State Materials and Technology Department filament winding center. The model can be either wire riding or free running with an installed autopilot. The hybrid motor uses nitrous oxide as oxidizer and burns cellulose. Even though it has a lower total impulse than the conventional motor, the hybrid's combustion can be extinguished by cutting off the oxidizer flow. When operating free running, a sensor, connected to a low-cost piezo element gyro package, will be used to stop the oxidizer flow if the model is unstable. The control surface elevation is controlled by pneumatic piston pressure. The piston, associated pneumatic tubing and valves, and mechanical linkages have been tested and should meet the requirements at the highest projected speeds. One-degree of freedom with the cavitator and possibly rotation of two control surfaces will be controlled by electric servos. A four-channel data logger will record operational parameters. The ventilation gas will be supplied by a compressed gas cylinder, a quick opening valve and a constant flow rate valve.

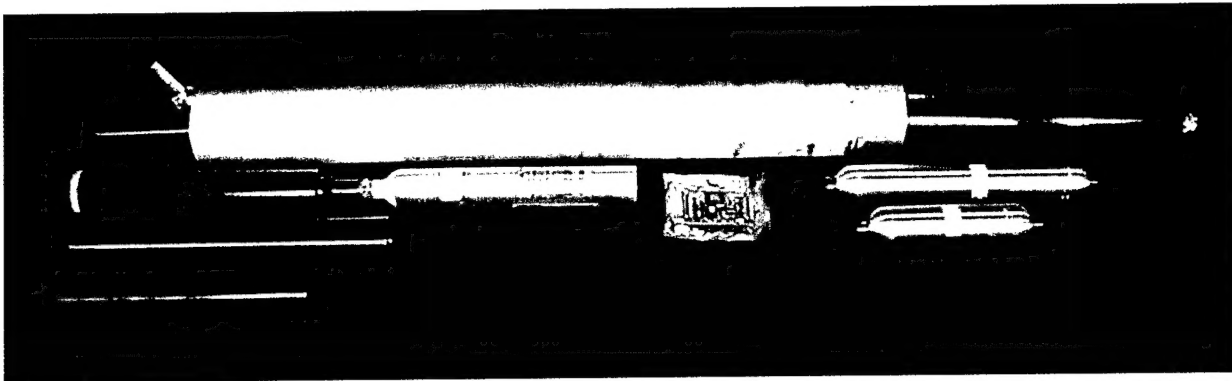


Figure 6: Photograph of 4-inch diameter 5-foot long powered model (not with composite shell) showing, conventional (red) and hybrid (black cylinder with oxidizer tank attached) motors, data logger (center), ventilation gas cylinders, and pneumatically operated control surface (mounted on aft region)

Flow noise associated with turbulent boundary layer (TBL) wall pressure fluctuations span wide ranges of temporal (frequency) and spatial (wavevector) scales. Basic issues and concerns for the new area of high-speed supercavitating bodies include:

Description of the wetted flow TBL wall pressure spectrum at low subsonic speeds. This issue arises because the Chase [1,2] theories assume incompressible flow, and the Maestrello [3] theory is based upon space-time correlation measurements made at Mach numbers greater than 0.3; the subject application is for $0.01 < M < 0.1$.

How does this spectrum change when a thin air layer exists between the wall and the high-speed water? No theory exists at this time to answer this question.

What implications do the higher Mach numbers and the presence of an air layer have on the balance between the non-propagating “pseudo sound” pressure fluctuation components and the low wavevector radiated noise components?

These issues are being addressed in this flow noise task.

In FY 1998, we concentrated on using some existing theories to predict wetted-flow TBL noise at speeds up to 200 ft/s ($M=0.04$) and compared these predictions to flow noise measurements obtained in the (empty) 1.5-inch Ultra-High-Speed Water Tunnel. Figure 7 shows a schematic diagram of this facility.

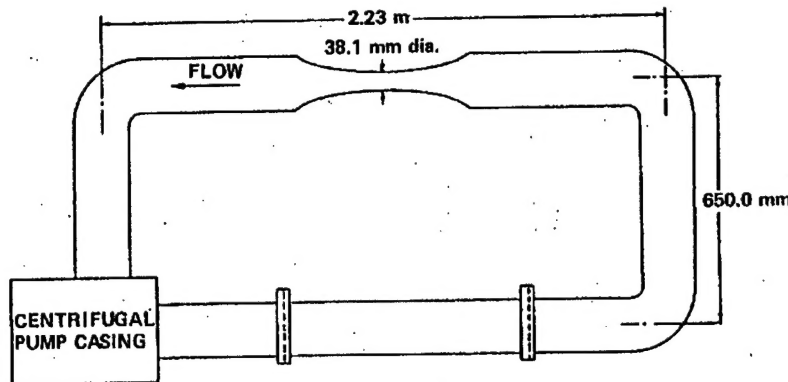


Figure 7: Schematic diagram of the 1.5-inch Ultra High-Speed Water Tunnel

The experimental wall pressure fluctuation data were acquired using a small wall-mounted piezoelectric pressure sensor. Figure 8 shows a typical experimental spectrum compared to some of the theories investigated thus far.

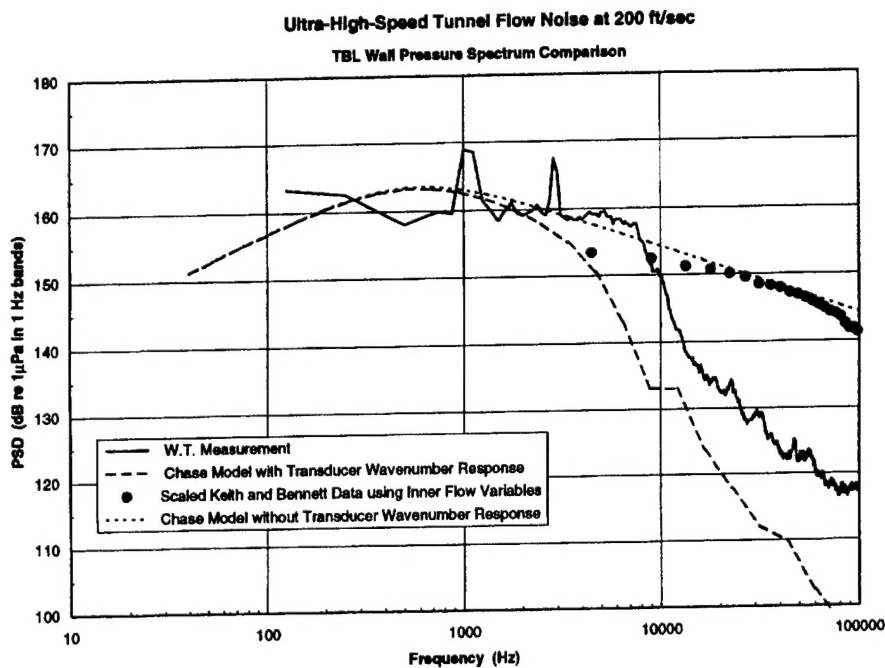


Figure 8: Wall pressure spectra measured and predicted for a location in the ultra-high speed water tunnel wall. This is for fully-wetted flow.

Keith and Bennett [4] report dimensionless wall pressure spectra measurements that were obtained in a developing channel flow of water at 20 ft/s. Although their data were measured using a single “point” transducer, the transducer diameter in terms of viscous wall units (denoted as d^+) was 430. Realizing that transducer spatial averaging effects may exist in their data, they corrected the spectra for these effects using the standard

Corcos correction scheme [5]. Upon scaling the Keith and Bennett spectra to the conditions of the high-speed water tunnel tests, we see that agreement to the actual experimental spectrum occurs only at very low frequencies; the high-frequency spectra diverge. This difference is likely due to water tunnel transducer spatial averaging effects. Because of the extremely high water speed, and because we used a measurement transducer of diameter 0.218-in, $d^+ = 10,600$. Obviously, the spatial averaging effects in the high-speed experiments are quite severe, and that should explain why the experimental spectrum diverges from the Keith and Bennett data, which is for a much smaller value of d^+ . To clarify this further, we integrated the theoretical Chase [2] wall pressure wavevector/frequency spectrum over all wavenumbers to get the fine broken-line spectrum of Fig. 8 that seems to agree with the Keith and Bennett data. No transducer correction was used in this integration meaning that the prediction is the estimate for a true point measurement.

The effect of the transducer spatial averaging can be accounted for, theoretically, by integrating a weighted form of the wall pressure wavevector/frequency spectrum over all wavevectors. The weighting function is the transducer wavevector response function. The details of this computation are presented by Capone and Lauchle [6] and the result is shown in Fig. 8 as the heavy broken-line spectrum. The spectral shape is predicted quite well, but there is still some high-frequency discrepancies when compared to the measurements. The reasons may be associated with non-flow related background noise in the tunnel. Tests are continuing, particularly over a wider range of speeds and static pressure, to address this hypothesis. There is also the concern that the empirical constants used in the Chase [2] model may not be appropriate for the Mach number of this test. So, several more sensitivity studies must be completed before we completely resolve this issue.

Progress has also been made in the design and fabrication of a test model for future experimentation in the 1.5-inch Ultra High-Speed Water Tunnel. This small-scale model has been designed to acquire "radiated" flow noise data in the water tunnel, with the pseudo noise components due to the tunnel wall TBL suppressed. The 0.5-inch diameter model is centered in the tunnel test section and is supported by a sting mount in the tunnel diffuser. The design includes a single pressure transducer located at the forward stagnation point of the elliptical-shaped nose cap of the model as shown in Fig. 9. The nose transducer is a spherical piezoceramic crystal developed by the Materials Research Laboratory (MRL) at Penn State as part of an ONR MURI in Acoustic Transduction: Materials and Devices. The Co-Principal Investigator (GCL) is involved in this MURI which has enabled this leading edge transducer research to be applied to the current project in an efficient and timely manner.

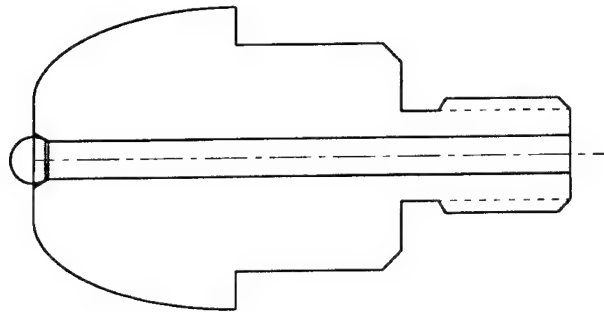


Figure 9: Sketch of the 0.5-inch diameter modified ellipse nose contour to be used in the future water tunnel tests. The small spherical ball at the forward stagnation point is the acoustic transducer that will sense radiated noise components, but not pseudo noise components that exist under TBL's.

Period of 1 December 1998 to 30 November 1999

Variable cavitator

The variable cavitator concept shows promise for a low flow noise, low drag/ large aperture cavitator to be used with a water reactive propulsion system. Adjustment of the center body position changes the drag and cavity shape allowing for increased maneuverability. A photograph of the variable cavitator test model used this past year is shown in Figure 10. The movable center body position is controlled by the water flow rate through an internal venturi. The position of the center body is adjusted by changing the flow rate of ingested water, which causes a pressure difference between the forward facing section of the center body and the internal/ aft facing section. If there were no water flow, the pressure in the venturi area would be stagnation pressure. This is higher than the pressure on the forward face, which in turn forces the center body out. As the water flow is increased, the velocity in the venturi increases and the pressure decreases. During normal operations, the pressure in the venturi section would be slightly higher than the pressure on the forward face to keep the center body extended. For large maneuvers, the water flow is increased by opening a valve in the propulsion system. This causes a decrease in the venturi pressure, and the center body retracts. The increase in the drag with the retracted center body increases the cavity size and allows for increased movement of the vehicle for turns.

It may be possible to design the system so that the increased thrust available from the increased water flow counteracts the increase in drag. The vehicle would then maintain speed in turns. This may be important in keeping the required total pressure head for the water reactive propulsion system. Small turns could be made with the center body extended. An added benefit for this system design is that there are no mechanical actuators required for center body movement. This can help with the vibration isolation of the center body from the rest of the vehicle, reducing array self noise.

Water tunnel tests this year demonstrated operation with the water flow venturi to control the center body position, Figure 11. The outer ring was changed from the design of the previous year. The lower drag wedge shape of the ring provided an increased change in the cavity size from the extended to retracted positions. There was also a greater change in the axial location of cavity inception as seen in the photographs. With partial retraction of the center body there were interim cavity shapes.

The center body position could be controlled quite accurately by adjusting the ingested flow rate. Water ingestion slot size, tunnel speed, and tunnel static pressure effects on the cavitator operation were investigated. A minimum retraction of the center body was found where the pressure differential was just sufficient to provide movement. Since the movement of the center body changes the drag, the ventilation gas flow requirements for the resulting cavity also change. These gas flow requirements effects on the cavity stability were examined. A number of modifications to the gas deflector system were required to provide smooth cavity transitions for the cavitator operating range.

For the fully extended center body position it was noticed that there were instabilities along the cavity wall, Figure 11. The cavity instabilities are similar to those seen during previous water tunnel tests with disk ring cavitators, where a boundary layer separation on the forebody reattached on the cavity. This will be examined with further tests next year.

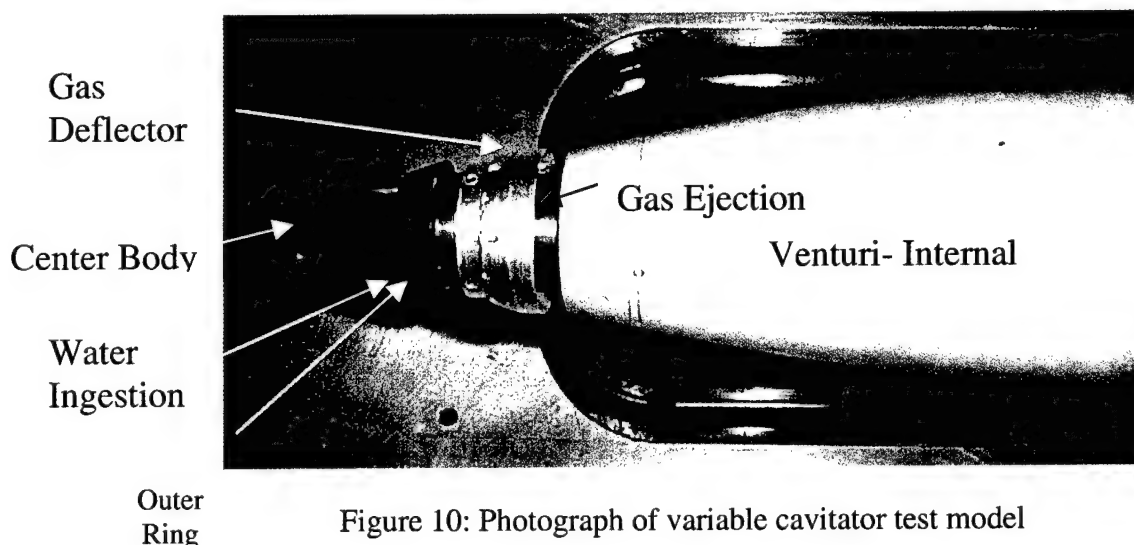


Figure 10: Photograph of variable cavitator test model

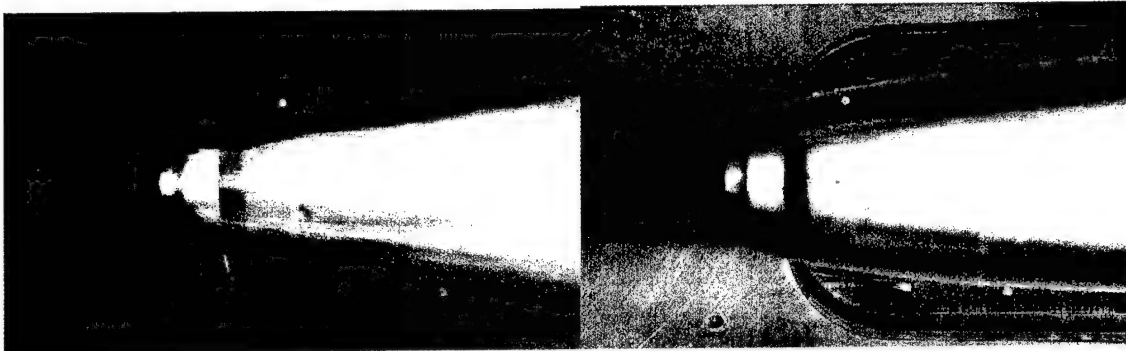


Figure 11: Photographs of water tunnel tests of the variable cavitator with the center body extended (left) and retracted (right)

Propulsor/ cavity interactions

Current theories can predict the shape of a cavity behind a cavitator to reasonable accuracy. However, the effects of high velocity exhaust from a propulsion system on the cavity shape, and in particular the cavity closure were not known. The primary objective of these water tunnel tests is to document the interaction of the propulsor exhaust on a ventilated cavity over a model travelling at high speeds. Two parallel wires were strung along the centerline of the upper leg of the ARL 48-inch diameter water tunnel, approximately 55 feet. Powered models ran along the wires, starting in the water tunnel settling section area, through the test section and ending in the settling section. The water level for the tests was two feet above the wires. The water level was then at the top of the test section and left air pockets above the water in the settling section and diffuser. These large air gaps reduced pressure rises due to the exhaust gases produced by the motor propellant. Hardware was designed to allow for ignition of the rocket motors under water. The model then traveled along the wires to the test section where the instrumentation was located. The primary instrumentation was video and high-speed movies to record the model and cavity. Transient wire tensions and radiated noise during the runs were also measured. After the models passed through the test section, they were stopped by using sliding disks on the wires. If a model came off the wires or if the wires broke, blast screen was used to protect the turning vanes at the end of the diffuser.

A photograph showing the major components of the models used for the tests is presented in Figure 12. An outer shell of graphite fiber composite holds the internal components. The four wire guides are soldered to stainless steel rings attached to the outer shell. The blue anodized aluminum tube has mounts for the rocket motor and ventilation gas cylinder. Attached to the gas cylinder is a quick opening valve, a shock bellows, and the tube that holds the gas deflector and cavitator.

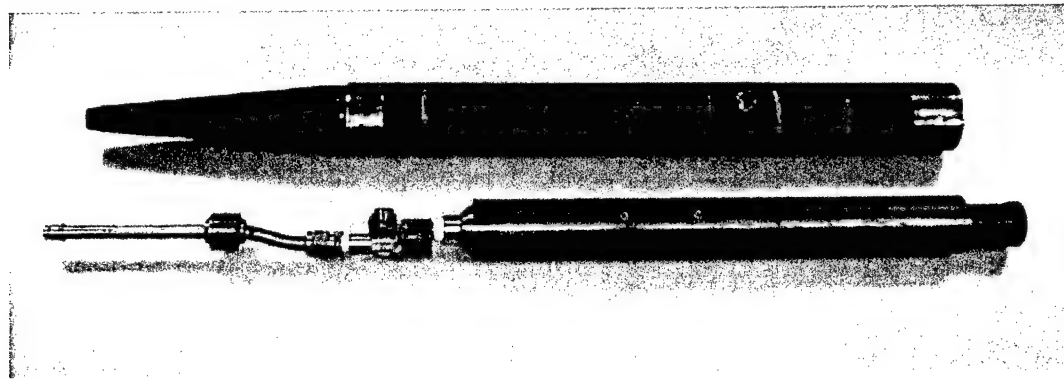


Figure 12: Photograph of the 2-inch diameter wire riding model showing the carbon fiber composite shell (above) and the internal components (below), ventilation system and propulsion motor

The motors used for the tests were 29 mm in diameter and manufactured by Aerotech™. The three size designations were G104T, H238T, and H220T. The G104T had a total impulse of 20.3 pound-seconds, a burn time of 0.9 seconds, and a thrust of approximately 25 pounds (at 0.5 seconds). The H238T had a total impulse of 39.4 pound-seconds, a burn time of 0.8 seconds, and a thrust of approximately 50 pounds (at 0.5 seconds). The H220T had a total impulse of 49.5 pound-seconds, a burn time of 0.9 seconds, and a thrust of approximately 55 pounds (at 0.5 seconds, peak thrust of 70 pounds). A photograph of one of the models installed on the wires is shown in Figure 13. The red cap at the end of the model is a cover to protect the motor nozzle prior to installing the igniter.

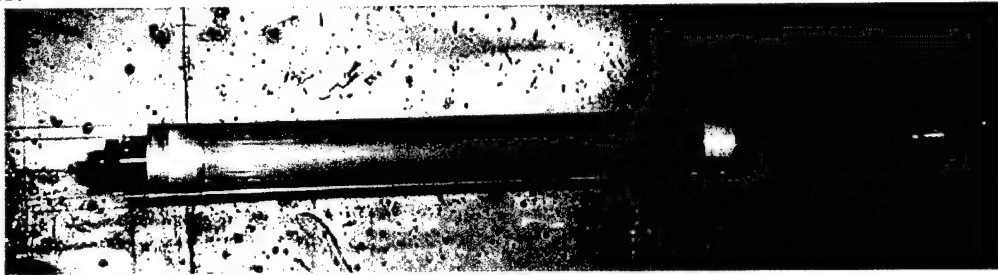


Figure 13: Photograph of the 2-inch diameter model installed on the wires in the ARL 48-inch diameter water tunnel

A photograph looking at the forward section of the model ready for launch is shown in Figure 14. The wires are tensioned with a worm gear winch shown at the bottom of the main I-beam support. Just above the winch are two turnbuckles, one on each wire, for equalizing the tension between the wires. Above the turnbuckles are two springs to maintain tension with the anticipated wire stretch. Above the springs are the load cells for measuring the wire tension. The wire tensions were set at 150 pounds per wire for testing. The transient wire tensions during a run were recorded at 500 points per second with a data acquisition system. The wires above the load cells were fed over two pulleys to be run down the tunnel. The model, ignition tube, and ignition tube support are also

seen in the figures. A second winch was used to hold the wires on the blast screen support at the other end of the tunnel.

All the instrumentation for recording the cavity behavior was located in the test section region of the tunnel. After passage through the test section, the models were stopped by sliding disks, as shown in Figure 15.

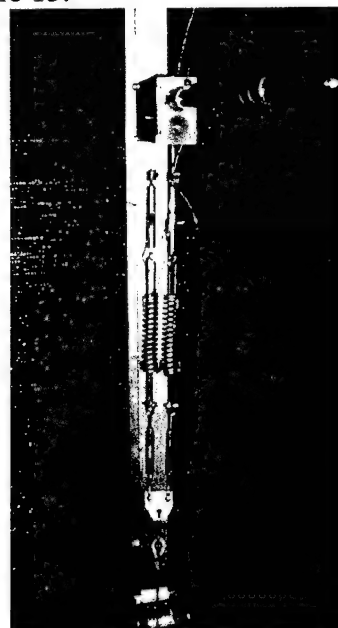


Figure 14: Photograph of the launch area showing the installed model, wire load cells and wire tensioning system

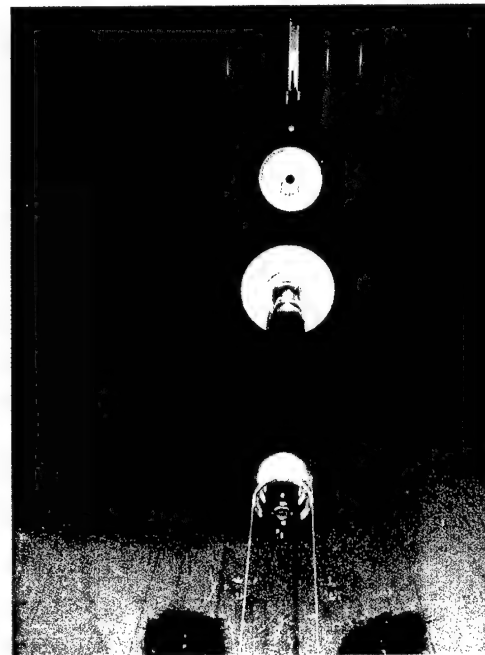


Figure 15: Photograph of the model retrieval area showing the model at a stopping disk with additional stopping disks in the background.

A total of 12 runs were made, with speeds ranging from 91 to 152 feet per second. Cavitator sizes of 0.407, 0.50, 0.60 and 0.70 inches in diameter were tested, and ventilation gas flow rate coefficients ranged from $CQ=0$ (no gas) to $CQ=0.82$. A number of gas deflector designs were also run.

A segment one of the high-speed movies with a ventilated cavity is shown in Figure 16. The exhaust plume and cavity closure region were measured and compared to the unventilated, baseline, case. After analyzing the data, it appears that the cavity "locks on" to the exhaust plume, which stabilizes the aft region of the cavity. It was also found that the minimum cavity/ plume size is governed by the gas entrainment and the plume blockage. A simple relationship, based on the propulsion exhaust volume flow rate, was developed and had a reasonably close agreement to the measured data. The results of this testing can be applied to provide estimates of the clearance between the aft region of a powered vehicle and the cavity wall.

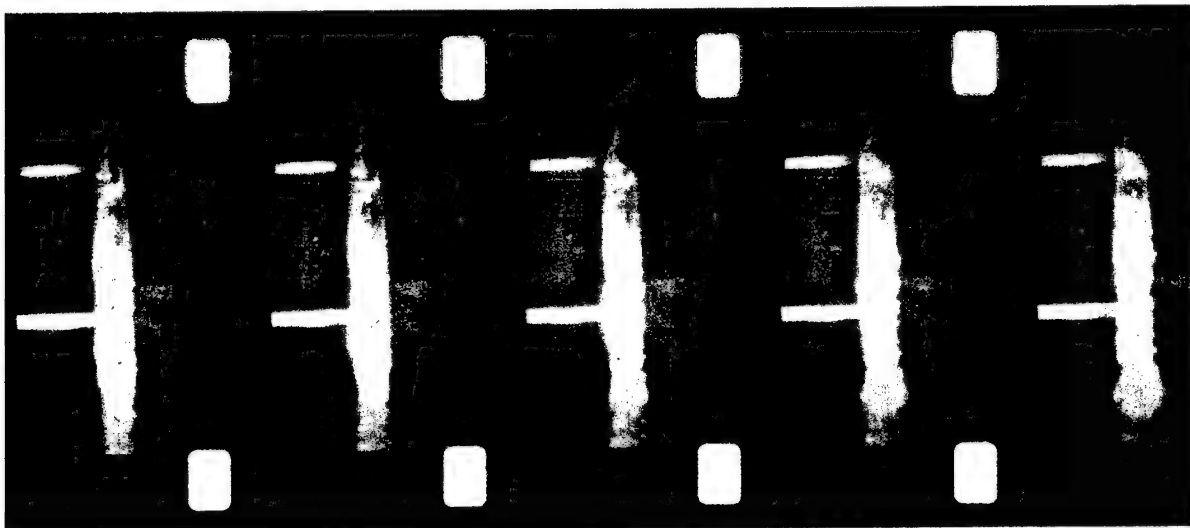


Figure 16: Segment from high-speed movie used for measuring the cavity/ exhaust plume interactions. Test #8, velocity=152 feet per second, $CQ=0.39$, 1000 frames per second

Cavity wall sensors

Knowledge of the body/cavity wall clearance is important as a diagnostic tool for the Test Bed and potentially to provide feedback for vehicle control systems. An electrical impedance technique was investigated for measuring the cavity wall position. With the electrical impedance method a low voltage, typically 1 volt, AC signal is applied to an electrode. The AC voltage reduces polarization effects of the electrodes. Additional electrodes are connected to JFET input precision op-amps. The electrical impedance between electrode pairs changes abruptly depending on whether there is water or gas over the electrodes. Such a system could be used for sensing the cavity position over a supercavitating vehicle. Since the aft control surfaces penetrate the cavity, they are a

logical location for the sensors. An electrode pattern to be used with a Test Bed fin is shown in Figure 17. The fins for the Test Bed are designed to be elevated with pneumatic actuators. The fin elevation angle is measured and is a function of the fin drag forces. In Figure 17, the center electrodes are the reference. By knowing the measured elevation angle and the adjacent electrodes signals, the cavity position and relative angle with respect to the body can be obtained. The lines drawn in the figure indicating some cavity wall location illustrate this point. The circuitry and sample electrodes have been built and bench tested. The time response of the system should be more than capable of measuring not only steady-state cavity geometry, but transient waves and bubbly void fraction along the cavity wall as well. Transient waves would be a continuous modulated signal, where a bubbly void fraction would be an intermittent signal. The spatial resolution would be a function of the electrode array pattern density.

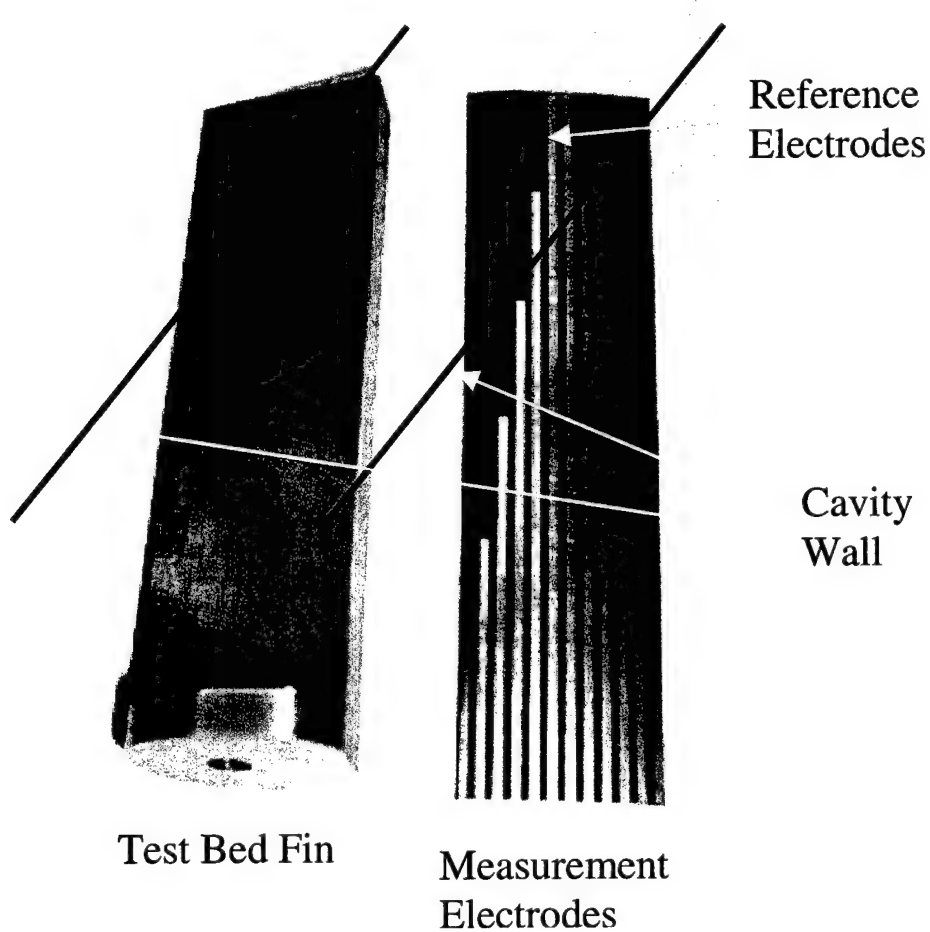


Figure 17: Photograph of test bed fin and cavity wall measurement electrode array

4-Inch diameter powered free running model

As part of the FY99 ONR 6.1 efforts, ARL built a 4-inch diameter powered-model to investigate basic scientific questions about high-speed bodies. Figures 18-21, show the 4-inch diameter 6.7-foot long powered vehicle with the hybrid motor. The model has a

forward pressure vessel that contains the ventilation system and cavitator actuator. The center pressure vessel contains the IMU and data loggers. The fins have pneumatic elevation from air cylinders near the motor. The hybrid motor uses a nitrous oxide oxidizer and a cellulose fuel. The exhaust products are nitrogen and hydrocarbons for an “environmentally friendly” system. The nitrous oxide flow will be controlled with a solenoid connected to the autopilot. The oxidizer flow can then be shut off if preset model limits are exceeded. Tentative plans are to have drag fins extend at end of run to slow the model. There will be redundant recovery systems. One will be a monofilament line payout similar to those used for “bow fishing”. The other will be a buoyancy bag inflated with a CO₂ cylinder, similar to those systems used by SCUBA divers. The bag will be wrapped around a phenolic tube over the “blast tube” area of the motor. The various components of the vehicle are low-cost and new configurations can be constructed in short periods of time in response to insights gained during operational tests. A unique feature of the proposed vehicle is its low cost per test.

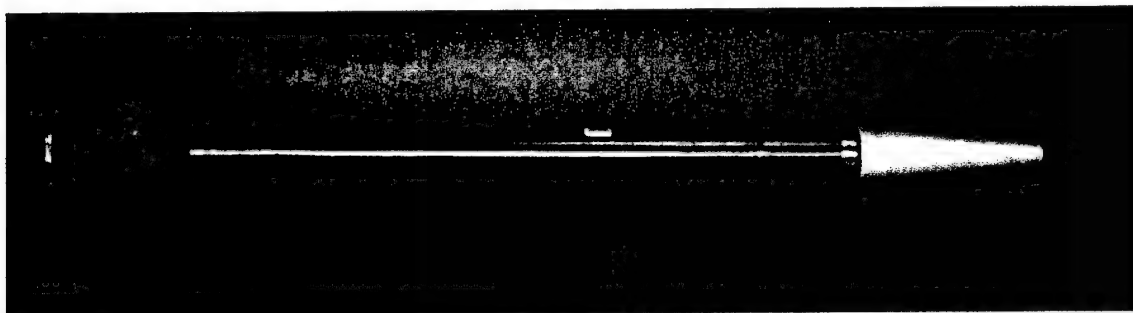


Figure 18: Photograph of the 4-inch diameter, 80-inch long free running powered model

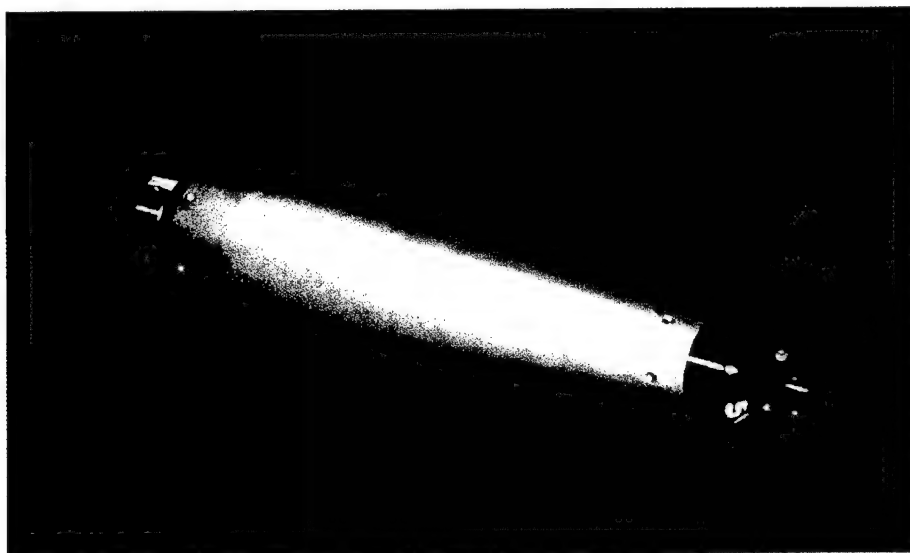


Figure 19: Photograph of the forward section of the model showing the cavitator and ventilation gas deflector

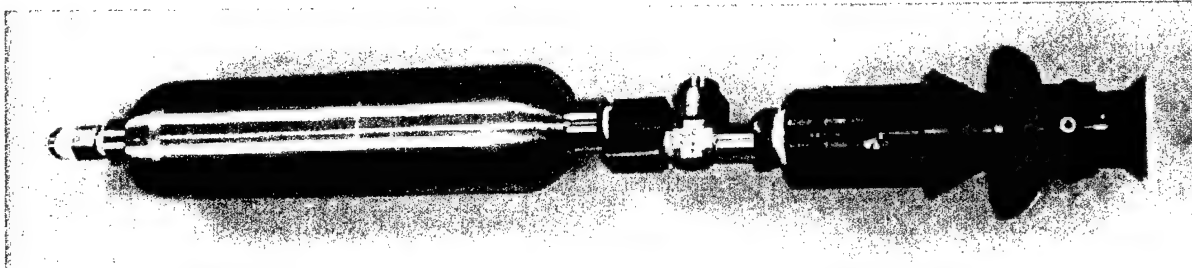


Figure 20: Photograph of the ventilation system showing the gas supply, gas valve, gas deflector and cavitator

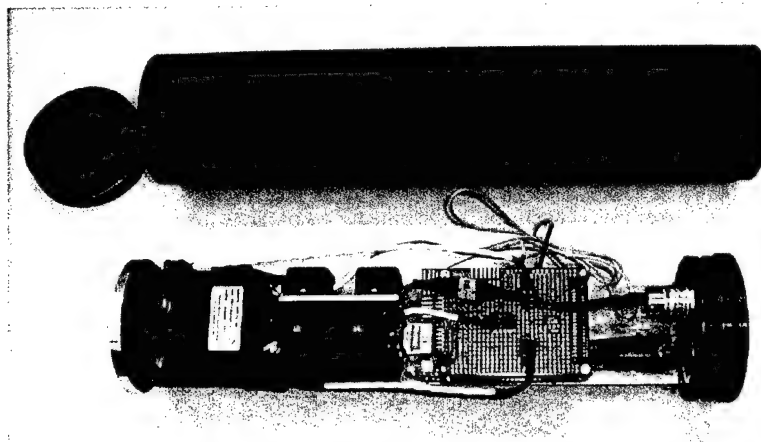


Figure 21: Photograph of inertial measurement package, data recorder and pressure vessel

Period of 1 December 1999 to 30 November 2000

Gas deflector design and cavity flow studies:

One of the major unanswered questions for the ONR Test Bed design is the required ventilation gas flow coefficient. Ventilation models have been proposed by team members where the average velocity of gas within the cavity is assumed to be close to the free stream velocity. With this assumption, the cavity/ body clearance must be small, or the ventilation gas flow rate must be very high for increased clearance. If there is significant recirculation of gas within the cavity, then the average flow velocity, and ventilation requirements are reduced. Recent calculations of the free stream and cavity flows, using the ARL UNCLE-M CFD code, are shown in Figures 22 and 23. The recirculation within the cavity is apparent in Figure 23. Results are similar farther downstream along the body. Also shown in Figure 22 are disturbances along the cavity wall due to the flow from the gas deflectors.

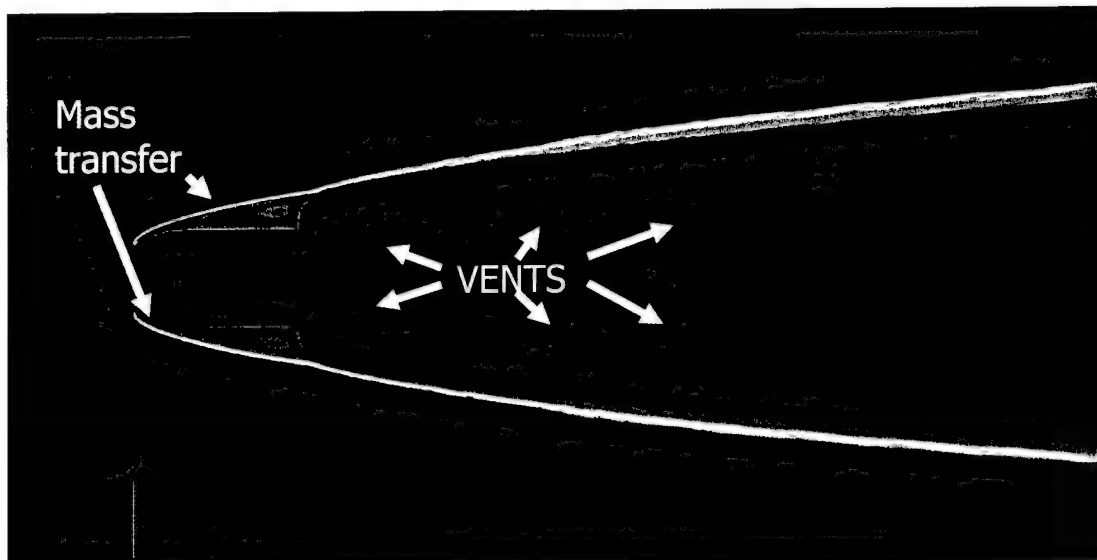


Figure 22: UNCLE-M calculation of density around a ventilated supercavitating body with three gas deflectors

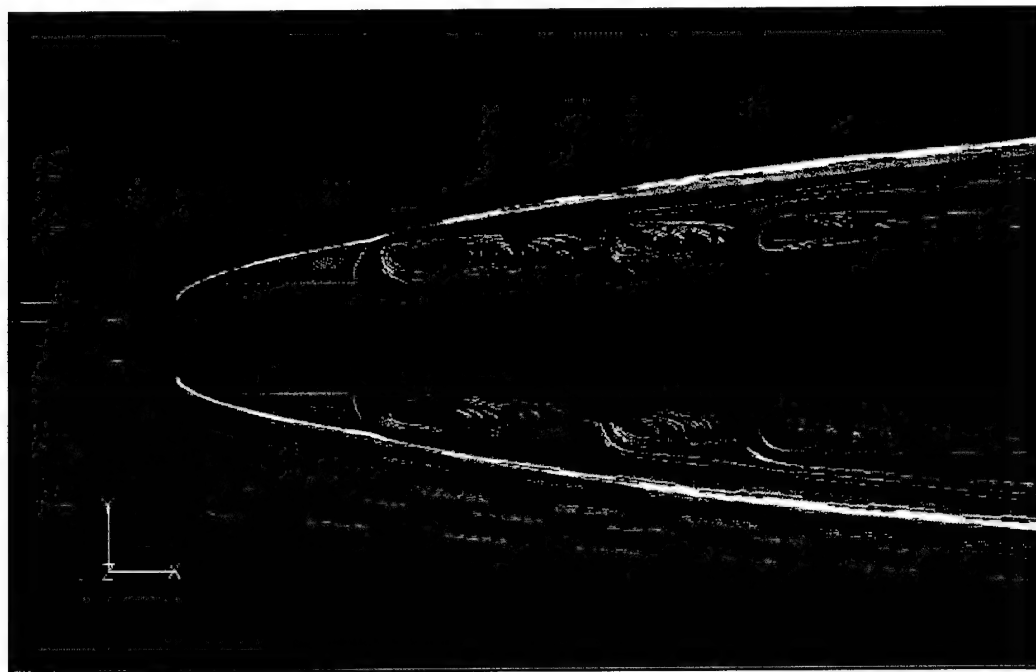


Figure 23: UNCLE-M calculation of the flows inside and outside the cavity

Tests are currently underway in the ARL 12-inch diameter water tunnel to study gas deflector design and flows within the cavity. Gas deflectors with equal radius of curvature and turning angles of 90, 80, and 70 degrees are being tested, Figure 24. The cavitators tested are a 1.39-inch diameter disk and a 2.285-inch diameter 20-degree half angle cone. These different geometry and sized cavitators are designed to have the same

drag. A 1.825-inch diameter 20-degree half angle cone is also being run. The cavitators/gas deflectors are compatible with the 4-inch diameter free running vehicle and the German Underwater Rocket. A photograph of the cavity disturbances from ventilation gas impingement is shown in Figure 25.

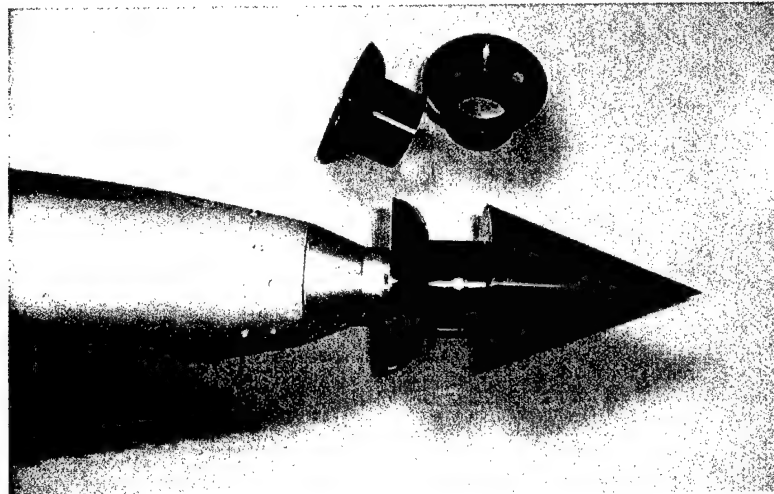


Figure 24: Photograph of the forward section of the model for testing gas deflector designs and studying flows within the cavity



Figure 25: Photograph of cavity disturbances due to ventilation gas impingement

Cavity wall sensors

Knowledge of the body/cavity wall clearance is important as a diagnostic tool for the Test Bed and potentially to provide feedback for vehicle control systems. An electrical impedance technique was investigated for measuring the cavity wall position. With the

electrical impedance method a low voltage, typically 1 volt, AC signal is applied to an electrode. The AC voltage reduces polarization effects of the electrodes. Additional electrodes are connected to JFET input precision op-amps. The electrical impedance between electrode pairs changes abruptly depending on whether there is water or gas over the electrodes. Such a system could be used for sensing the cavity position over a supercavitating vehicle. Since the aft control surfaces penetrate the cavity, they are a logical location for the sensors. An electrode pattern to be used with a Test Bed fin is shown in Figure 26. The fins for the Test Bed are designed to be elevated with pneumatic actuators. The fin elevation angle is measured and is a function of the fin drag forces. In Figure 26, the center electrodes are the reference. By knowing the measured elevation angle and the adjacent electrodes signals, the cavity position and relative angle with respect to the body can be obtained. The line drawn in the figure indicates some cavity wall location illustrate this point. The circuitry and sample electrodes have been built and bench tested. The time response of the system should be more than capable of measuring not only steady-state cavity geometry, but transient waves and bubbly void fraction along the cavity wall as well. Transient waves would be a continuous modulated signal, where a bubbly void fraction would be an intermittent signal. The spatial resolution would be a function of the electrode array pattern density.

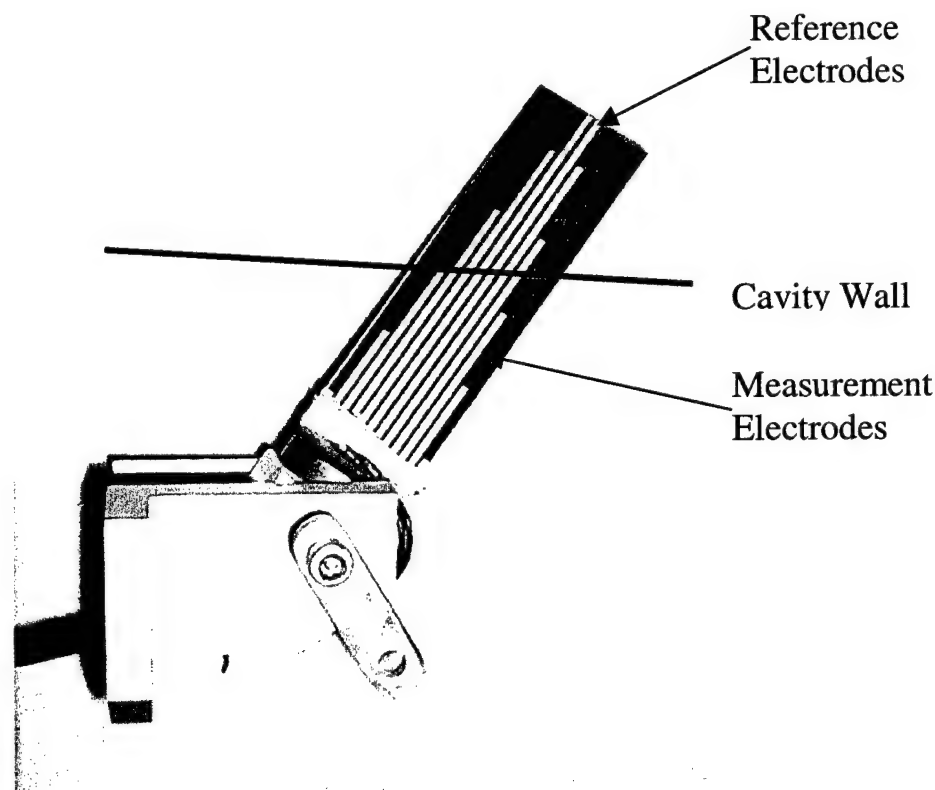


Figure 26: Photograph of test bed fin in water tunnel fin mount and cavity wall measurement electrode array

A wide range of electrode designs have been tested this past year. The electrode pattern shown in Figure 26 produces discrete signals as the cavity covers the electrodes. Ring electrodes along a body can be used to monitor the cavity development during the vehicle acceleration phase. Electrodes of this design have low electrical resistance. High resistance electrodes have been tested and operate in a different manner. The output signal of the high resistance electrode is proportional to the wetted area. This produces a continuous output signal. It is anticipated that both high and low resistance electrodes will be used for a range of cavity monitoring and vehicle control functions.

High speed flow noise

As part of the ONR 6.1 efforts, ARL built a 4-inch diameter powered-model to investigate basic scientific questions about high-speed bodies. Figures 27 and 28, show the 4-inch diameter 6.7-foot long powered vehicle with the hybrid motor. The model has a forward pressure vessel that contains the ventilation system and cavitator actuator. The center pressure vessel contains the IMU and data loggers. The fins have pneumatic elevation from air cylinders near the motor. The hybrid motor uses a nitrous oxide oxidizer and a cellulose fuel. The exhaust products are nitrogen and hydrocarbons for an “environmentally friendly” system. The nitrous oxide flow will be controlled with a solenoid connected to the autopilot. The oxidizer flow can then be shut off if preset model limits are exceeded. The various components of the vehicle are low-cost and new configurations can be constructed in short periods of time in response to insights gained during operational tests. A unique feature of the proposed vehicle is its low cost per test.

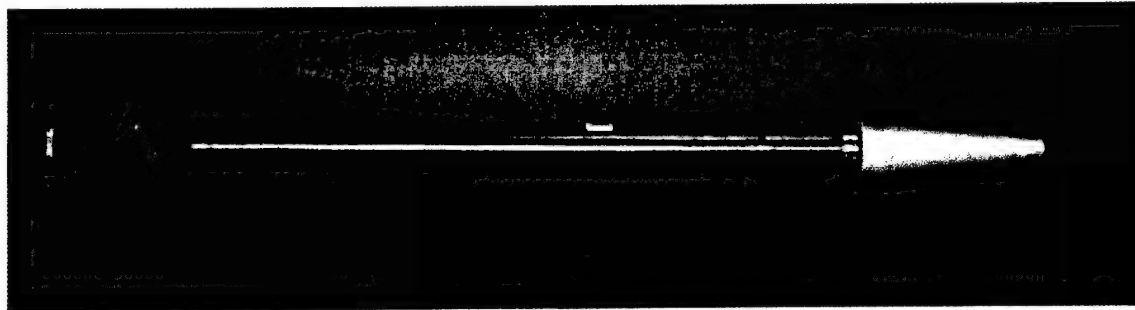


Figure 27: Photograph of the 4-inch diameter, 80-inch long free running powered model shown with fixed cavitator

Details of the forward sections of the model are shown in Figure 28. The array is being built by Bob Marciak's group under 6.2 funding. The array is vibration isolated from the vehicle structure by acoustic damping material at three locations. The array high speed data recorder is a custom unit and is located in the IMU section of the model. The recorder operates at 150 k Hz for up to 25 seconds and is started by an accelerometer at launch.

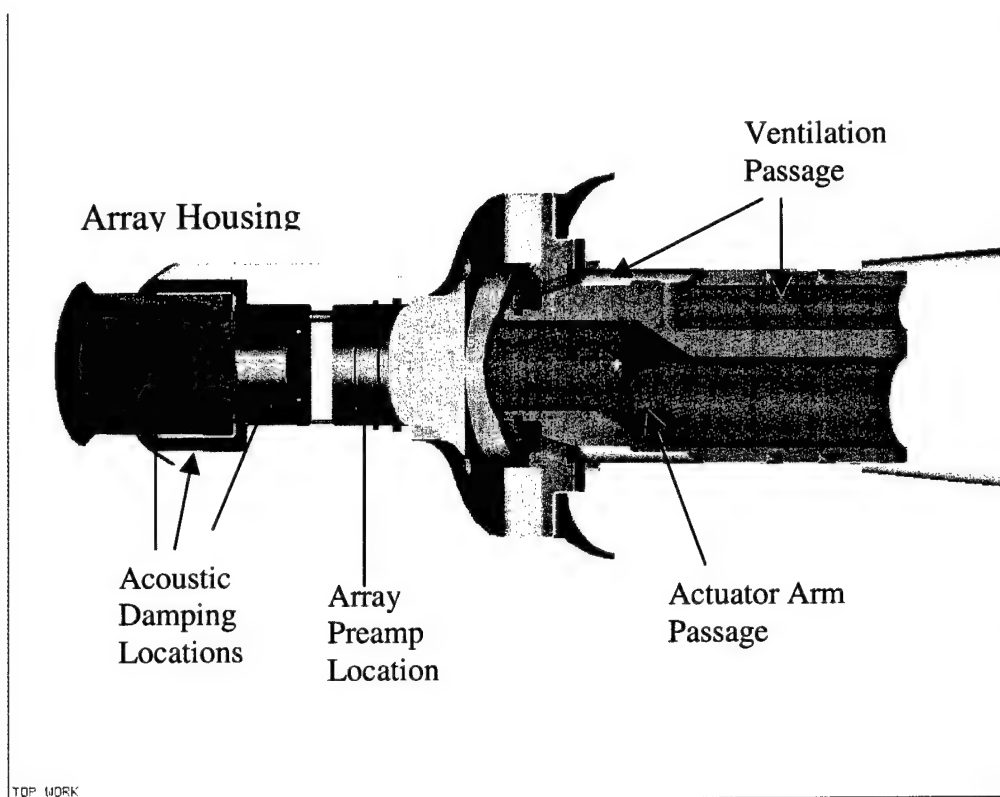


Figure 28: CAD drawing of forward sections of model with articulated cavitator showing array housing, actuator arm passage and ventilation passage

In June, a visit was made to the Aberdeen Test Center to arrange for tests in the UNDEX Test Facility. The UNDEX (Superpond) appears to be ideally suited for the types of tests that are planned. The launcher will be lowered from a barge to the desired launch depth, and will rest on a fixture attached to the barge. The pneumatic valve, initiating launch, will be operated from the barge. All model on-board systems are actuated by the launch acceleration. A standard operating procedure is being prepared for the Test Center. Current schedule is for testing in October.

Tip vortex studies

An important issue in bi-static homing is the link between the vehicle and host platform. One potential method for this link is with a fiber optic cable. However, the fragile nature of the fiber makes payout at supercavitating vehicle speeds difficult. It may be possible to payout the fiber into the gas filled tip vortex of one of the supercavitating control surfaces. A photograph of a water tunnel test of a Test Bed supercavitating control surface is shown in Figure 29. As shown in the figure, at high angles of attack there is a well-formed tip vortex. It may be possible to direct a fiber optic fiber along the control surface suction side and into tip vortex. The payout is in the ventilation gas until the fiber touches the tip vortex cavity wall. If the velocity of the fiber closely matches the velocity along the cavity wall there will be lower stresses in the fiber. It is possible that the lift-induced velocity will keep the vortex away from the vehicle propulsion exhaust.

The basic research issues for the control surface tip vortex that are being studied are,

- calculate the vortex centerline position downstream as a function of vortex strength,
- estimate the velocity components along the cavity wall near the control surface as a function vortex strength, and
- address vortex breakdown and vortex wandering.

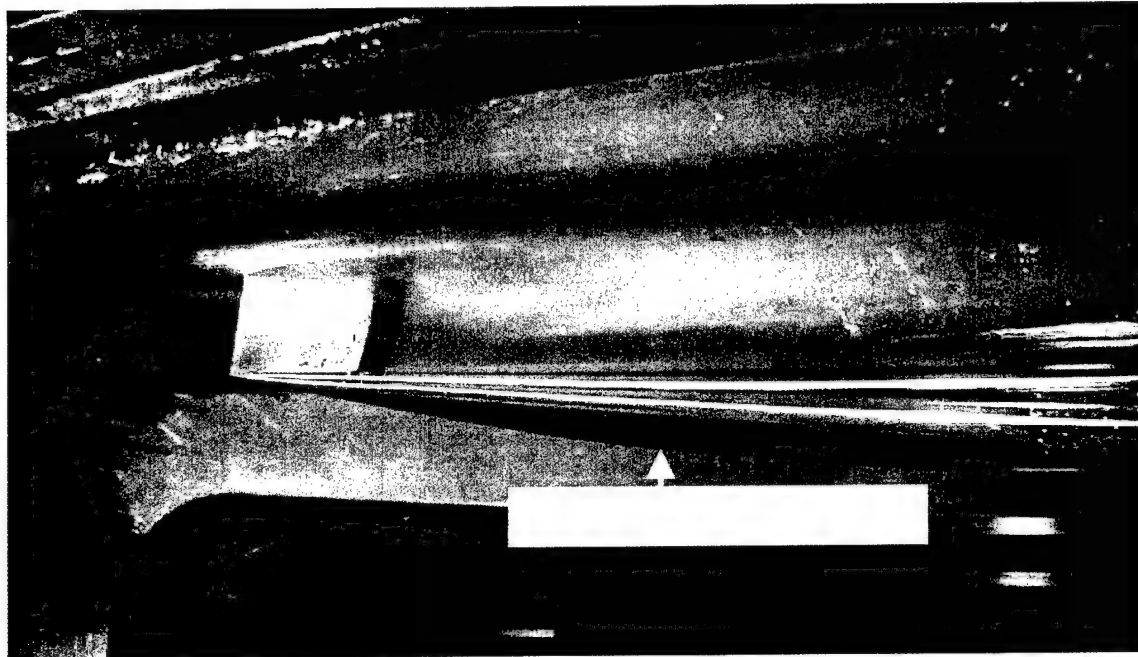


Figure 29: Photograph of a water tunnel test of a Test Bed supercavitating control surface showing the stable tip vortex

Period of 1 December 2000 to 29 June 2001

Cavity flow studies

One of the major unanswered questions for vehicle design is the required ventilation gas flow coefficient. Ventilation models have been proposed by team members where the average velocity of gas within the cavity is assumed to be close to the free stream velocity. With this assumption, the cavity/ body clearance must be small, or the ventilation gas flow rate must be very high for increased clearance. If there is significant recirculation of gas within the cavity, then the average flow velocity, and ventilation requirements are reduced. Calculations of the free stream and cavity flows, using the ARL UNCLE-M CFD code, show recirculation within the cavity.

Last year tests were conducted where smoke was mixed with the injected ventilation gas to study mixing and recirculation within the cavity, Figure 30. From the results shown in the figure it appears that there is no smoke near the edge of the cavity, indicating dissipation by mixing. However, this is an illusion caused by the index of refraction of

water and the gas-filled cavity. Tests will be conducted in the next few weeks with smoke ejection downstream of the primary ventilation location. Recirculation within the cavity will be indicated by migration of the gas upstream.

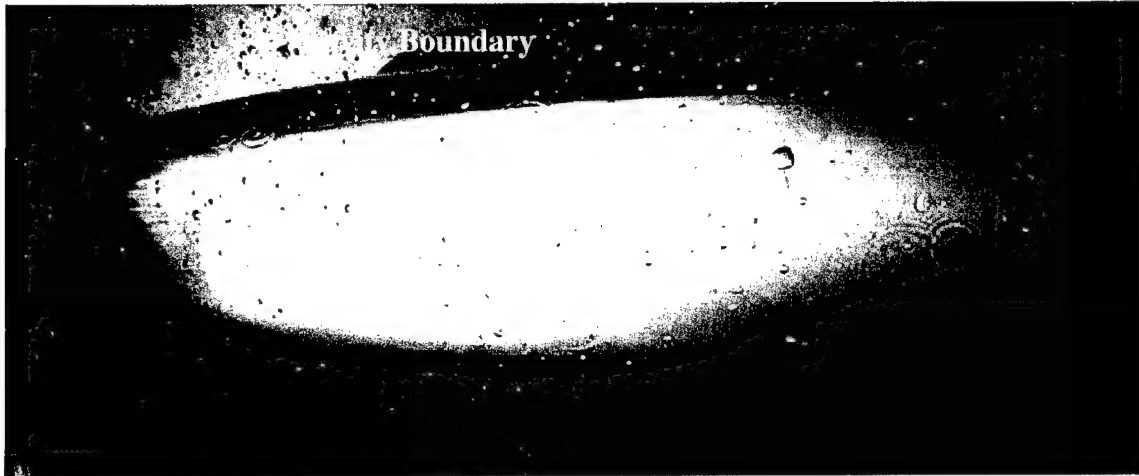


Figure 30: Photograph of cavity with smoke/ ventilation gas mixture

Cavitation Optimization for Minimizing Flow Noise

A primary objective of the supercavitation research is minimizing flow noise to maximize acoustic array performance. The hydrodynamic design of the cavitator is critical in not only generating a stable cavity over the body, but also in maintaining a laminar boundary layer for the range of operating conditions. Last year at the workshop, data for 20-degree half-angle cones was presented that showed perturbations to the cavity which correlated with calculations of boundary layer stability, Figure 31. The cavity generated by the cone was used as a flow visualization technique to show the perturbations. One reason for studying this particular cone geometry is that the Germans use it for their underwater rocket. During the April/ May 2001 tests of the German model, it was noticed that as the cavitator was slewed, other disturbances were seen on the upstream edge of the cavity. It is very likely that the flow is separating into two vortices shed from the cone at angle of attack. This would result in a significant increase in flow noise. The Germans also mentioned they had only achieved approximately 30% of the predicted acquisition range for their acoustic array.

A model is being built for diagnostic measurements of slewing cavitators using Particle Image Velocimetry (PIV). PIV will be used to obtain velocity field "snapshots" about cavitators. Boundary layer transition, separation and reattachment can be measured.



Figure 31: Photograph of cavity disturbances due to boundary layer perturbations

Free Running Vehicle- Hydrodynamics and Flow Noise

As part of the ONR 6.1 efforts, ARL built a 4-inch diameter free running model to investigate basic scientific questions about high-speed supercavitating bodies in a free-field environment. The first tests of the model were completed at the Aberdeen Superpond, 11-14 June 2001. These first series of tests at Aberdeen are being conducted with an impulse launched model and no propulsion. The objectives are to investigate cavity ventilation requirements, cavity stability, body stability and baseline flow self noise. Later tests with the propulsion system will show changes to the baseline configuration. A photograph of the model as recovered after Test#2 is shown in Figure 32. Figure 33 shows the launcher being positioned on the barge and Figure 34 is the launcher below the water and mounted to the side of the barge.

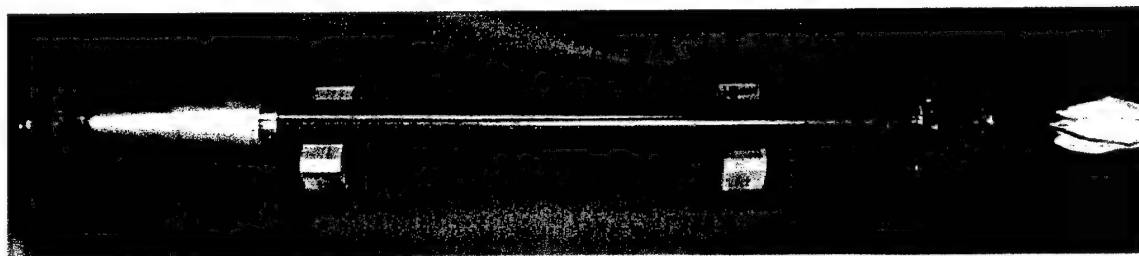


Figure 32: Photograph of the 4-inch diameter, long free running model shown with recovery chute deployed, after recovery at Aberdeen

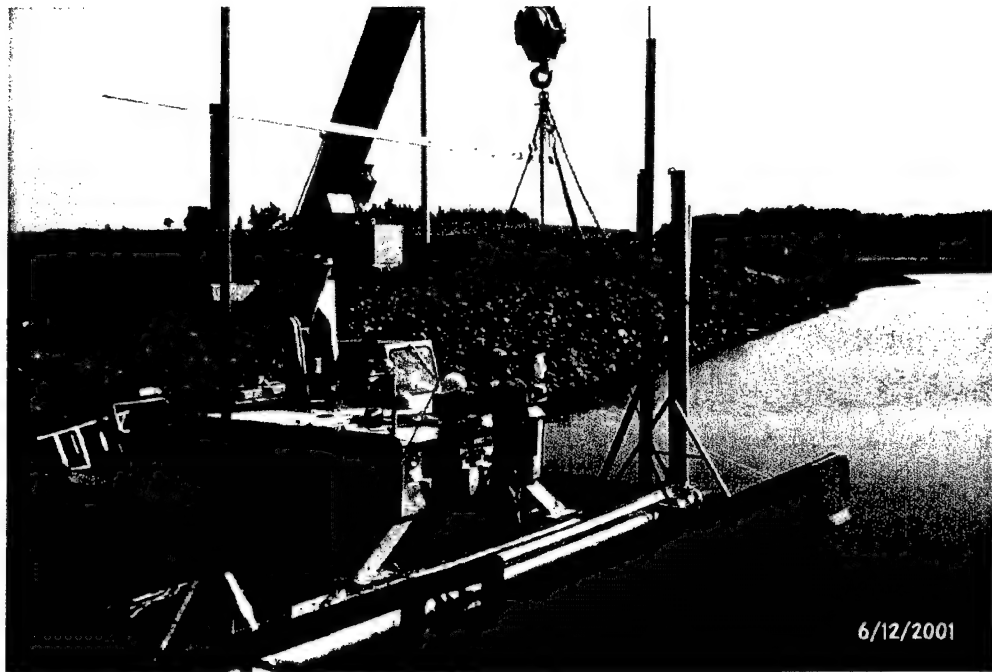


Figure 33: Photograph of the launcher being lowered over the side of the barge

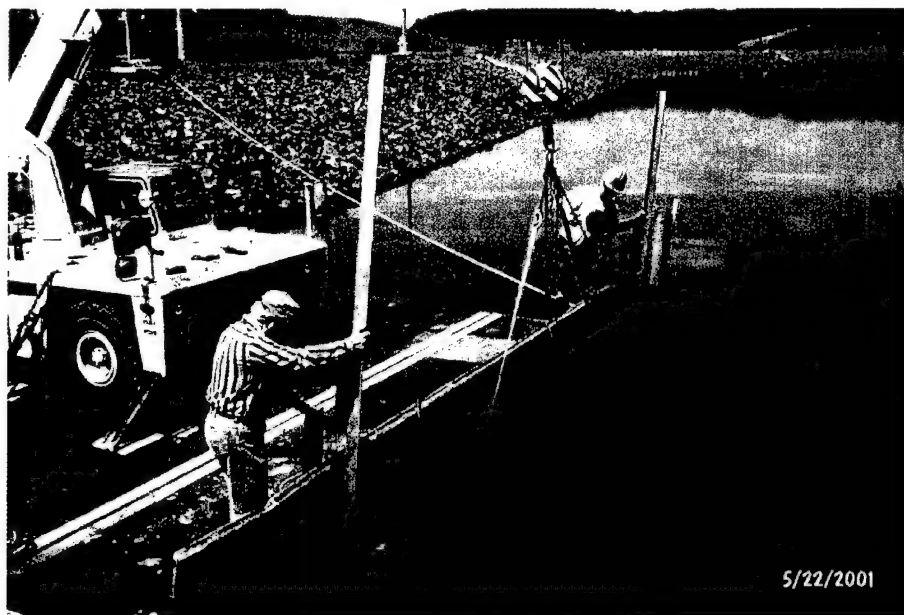


Figure 34: Photograph of the launcher submerged with the vent tube above the surface

The current configuration allows fixing the cavitator at a specific angle using mounting blocks as shown in Figure 35. A metal bellows seals between the cavitator housing and the forward section of the model for passage of the electrical leads for the acoustic array and for linkage to a cavitator actuator, when installed, Figure 36. The ventilation system consists of a pressurized cylinder, a trip valve system, metering orifice, and gas deflector. The pressurizing cylinder is filled to 1500 psi with the trip valve closed. The acceleration

of launch opens the valve where the gas passes through the metering orifice. The metering orifice size is determined by the required peak gas flow rate based on the launch velocity and ventilation flow coefficient. A nearly constant ventilation flow coefficient is assumed since the exponential decrease in gas flow from the cylinder should match the exponential velocity decay (assuming constant drag coefficient for the critical part of the run). There are a number of metering orifices to cover a range of tests conditions. The ventilation gas exits the model through the gas deflector as shown in the Figure.

The IMU modules are located just aft of the forward cone and are described in the ONR 6.1 proposal by John Dzielski.

The fin subsystem consists of a pressurized cylinder, a spool valve, pneumatic elevation cylinders, and the fin mounts. For the current runs, two fins were located at 45 degrees from top dead center. Fin elevation is controlled through a pressurized cylinder and a spool valve. The pressurized cylinder is filled to a pressure that controls the elevation torque to the fins. Prior to launch the fins are in the "retract position". At launch, the acceleration opens the spool valve between the pressurized cylinder and the pneumatic elevation cylinders. At the highest velocity, at launch, the fins "lean back" due to the hydrodynamic forces. As the velocity decreases the fin elevation increases. The fin's wedge shaped cross section had a half-angle of 10 degrees. The angle of attack for both fins was fixed at 10 degrees in the direction to provide lift to the aft section of the model. This angle of attack was chosen for maximum fin cavity stability for the full range of the test.

The recovery system consists of an electronic timer, solenoid, trip valve, pressurized cylinder, parachute, and float with recovery line. The acceleration at launch starts the electronic timer. After a specified time (2 seconds for run #1 and 3 seconds for run #2) a pulse is sent to the solenoid that trips the valve to the pressurized cylinder. The air from the cylinder ejects the parachute slowing down the model. The float, with line attached, pays out and indicates the model location. Model recovery is by pulling up the model with the line.

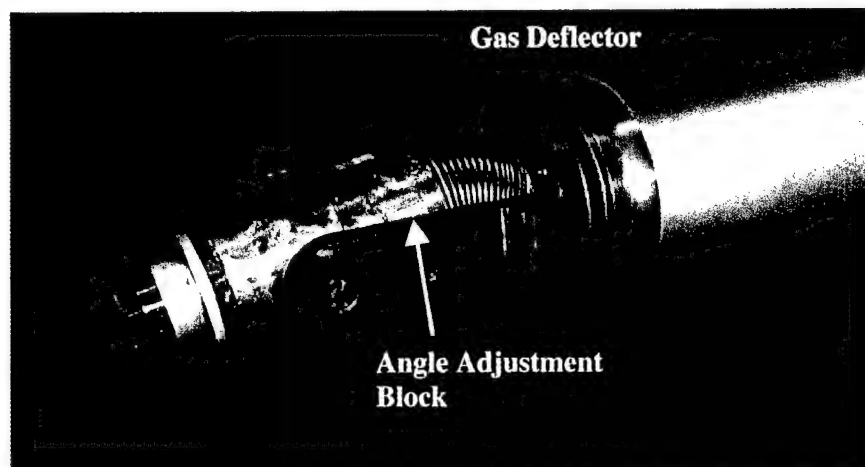


Figure 35: Photograph of the forward section of the model

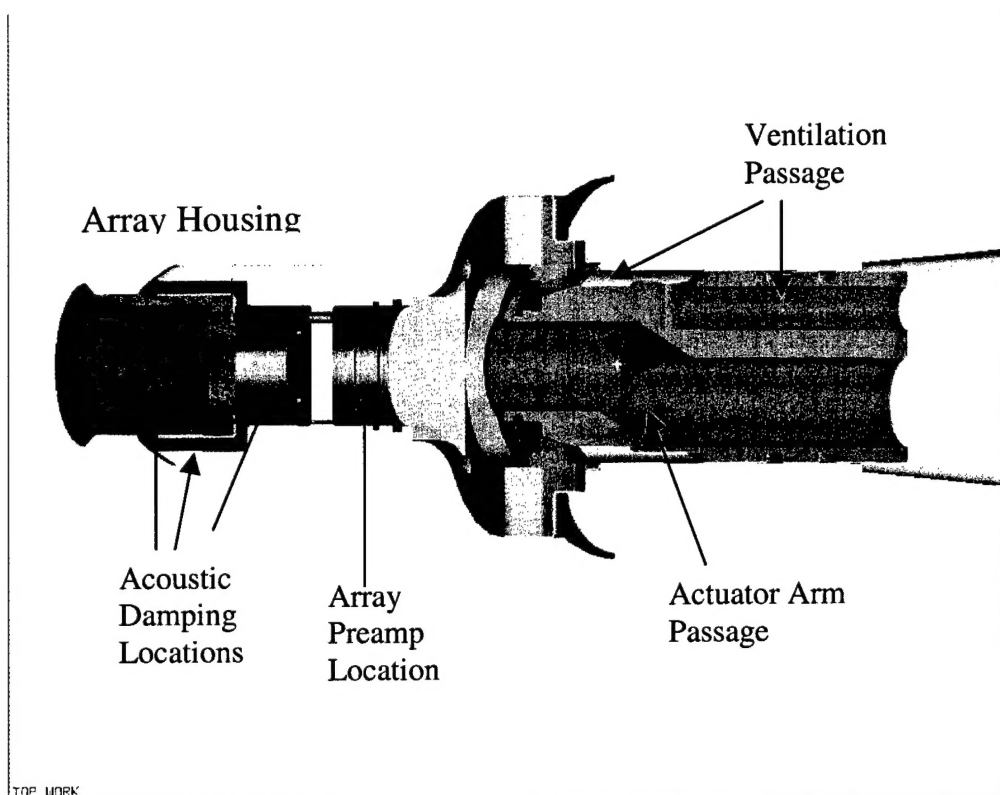


Figure 36: CAD drawing showing detail of nose

A “pusher” as attached to the aft section of the model prior to installation in the launcher. This pusher protects the model from the high ejection pressures. The model is installed in the launch tube and the end sealed with a rupture diaphragm, a cellophane-like material. The pneumatic valve pressure vessel is filled to 125 psi maximum. The launcher is then lowered below the water surface and hung from the side of the barge with brackets. The launch main pressurizing tube is filled through a line connected to a pressure cylinder and regulator, 125 psi maximum pressure. At launch, the pneumatic valve, between the main pressurizing tube and launch tube, is opened. The model is propelled down the launch tube by the air pressure. Air in front of the model escapes through the vertical tube that extends above the water surface. The model exits the launcher by passing through the rupture diaphragm. The speed of the model is controlled by the pressure in the pressurizing section and the rate of the valve opening. Videos of the model trajectory are made with a camera in a waterproof housing below the surface and with a camera above.

There were two runs during the first series of tests at Aberdeen. The IMU data and vehicle trajectory are discussed in the proposal submitted by John Dzielski. Based on the underwater camera records, the cavity was larger than required for optimal vehicle stability. A conservative ventilation coefficient of $CQ = 1.0$ was chosen to ensure a cavity over the model. The next series of tests will be conducted with lower ventilation gas flow rates. The first run, at lower impulse launch pressure, went straight and all components appeared to function correctly. The second run, at higher impulse launch pressure,

veered left after leaving the tube. It was discovered that the high launch acceleration caused the drag chute to deploy as it exited the tube. This resulted in the short range and likely contributed to the errant trajectory. A simple fix has been designed to prevent this from occurring on future launches. The next series of tests are scheduled for the week of 6 August.

Details of the forward sections of the model are shown in Figure 36 and a photograph of the acoustic array is shown in Figure 37. The array is being built by Bob Marcinia's group under 6.2 funding. The array is vibration isolated from the vehicle structure by acoustic damping material at three locations. The array high-speed data recorder is a custom unit and is located in the IMU section of the model. The recorder operates at 150 k Hz for up to 25 seconds and is started by an accelerometer at launch.

Array self-noise measurements with the ventilation system operating were performed in the ARL acoustic tank. The model was mounted so that the array was just below the water surface and the rest of the model in air, Figure 38. An axial accelerometer was attached to the cavitator housing ahead of any acoustic damping. The model's pressurized cylinder was filled to 1500 psi and released through a metering orifice.

Figure 39 shows the coherence between the array sum and the axial accelerometer during ventilation. The strongest correlation exists in the frequencies below 10 kHz.

Further component testing to assess the ventilation system acoustic and structure-borne contributions to array self-noise is planned - including ventilation system / gas ejection quieting techniques and advanced vibration isolation methods.

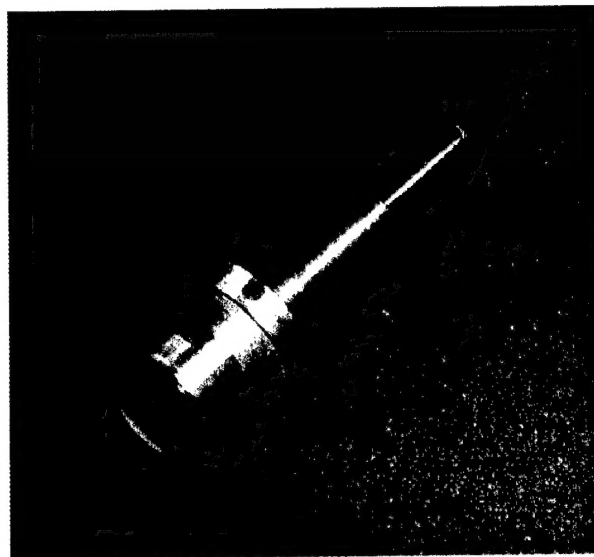


Figure 37: Photograph showing first planar acoustic array



Figure 38: Photograph showing mounting arrangement for self noise tests

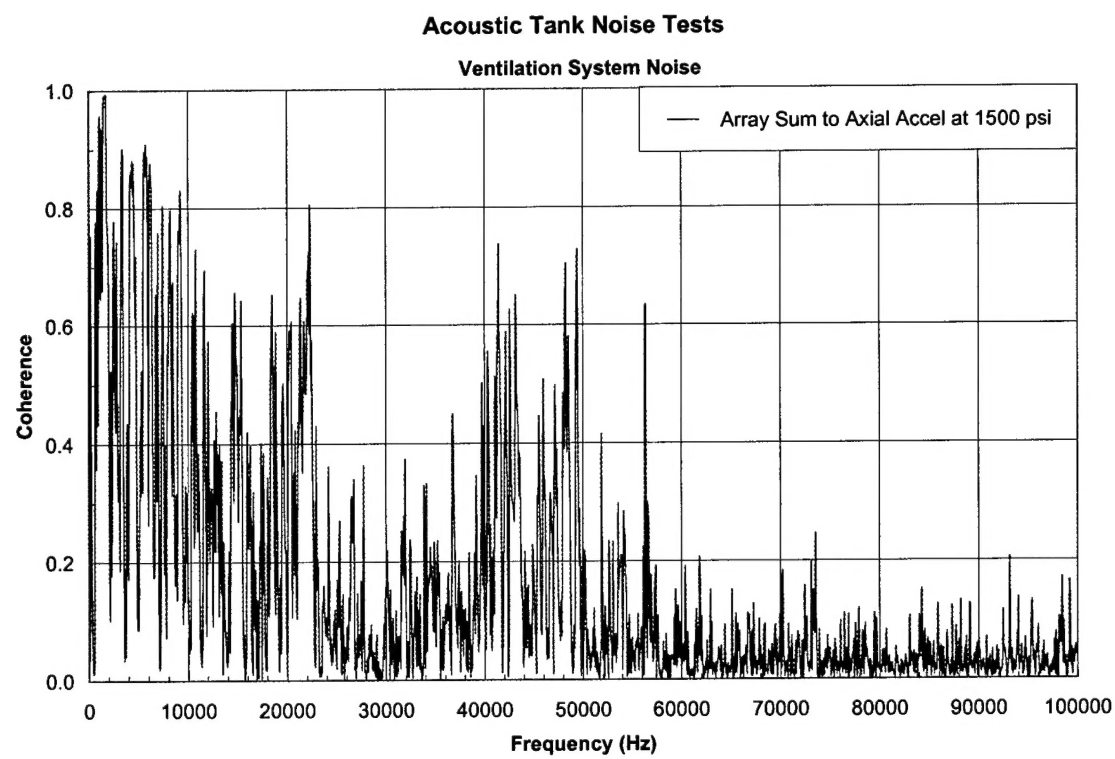


Figure 39: Coherence between the array sum and the axial accelerometer

Control surface hydrodynamics and tip vortex studies

An important issue in bi-static homing is the link between the vehicle and host platform. One potential method for this link is with a fiber optic cable. However, the fragile nature of the fiber makes payout at supercavitating vehicle speeds difficult. It may be possible to payout the fiber into the gas filled tip vortex of one of the supercavitating control surfaces. A photograph of a water tunnel test of a Test Bed supercavitating control surface is shown in Figure 40. As shown in the figure, at high angles of attack there is a well-formed tip vortex. It may be possible to direct a fiber optic fiber along the control surface suction side and into tip vortex. The payout is in the ventilation gas until the fiber touches the tip vortex cavity wall. If the velocity of the fiber closely matches the velocity along the cavity wall there will be lower stresses in the fiber. It is possible that the lift-induced velocity will keep the vortex away from the vehicle propulsion exhaust.

The basic research issues for the control surface tip vortex that are being studied are,

- calculate the vortex centerline position downstream as a function of vortex strength,
- estimate the velocity components along the cavity wall near the control surface as a function vortex strength, and
- address vortex breakdown and vortex wandering,
- measure forces generated by control surfaces.

A model with a fin elevation torque cell will be tested in the 12-inch water tunnel.

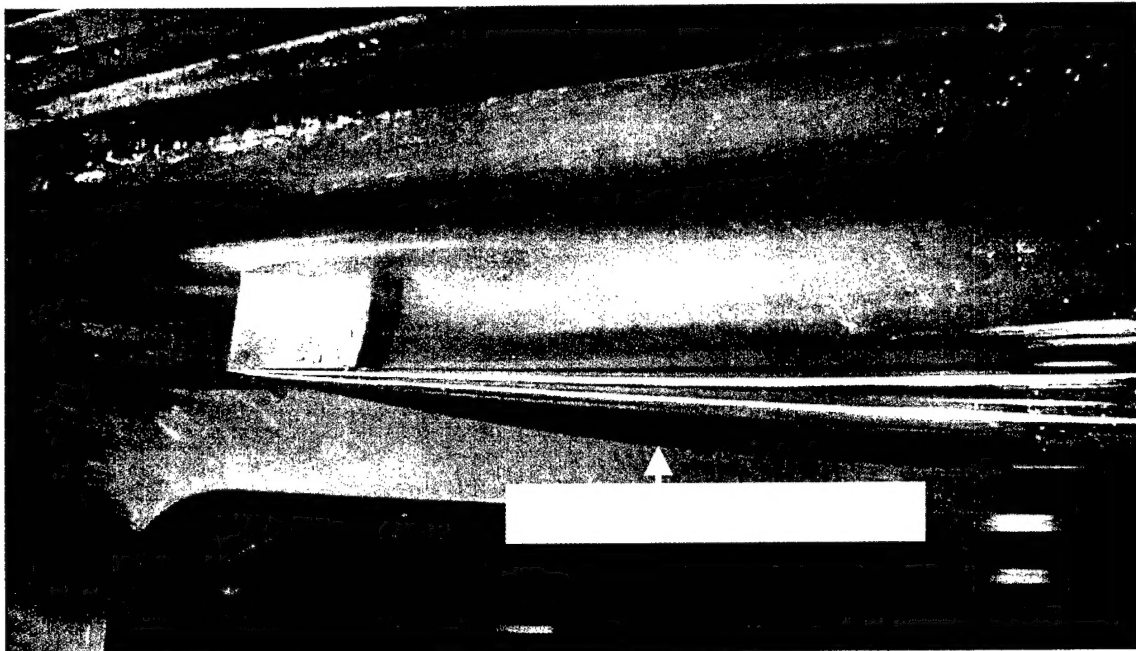


Figure 40: Photograph of a water tunnel test of a Test Bed supercavitating control surface showing the stable tip vortex